

Nonlinear resonance in barotropic-baroclinic transfer generated by bottom sills

Julia Boschan,¹ Miklós Vincze,^{1,a)} Imre M. Jánosi,¹ and Tamás Tél^{1,2}

¹*von Kármán Laboratory for Environmental Flows, Institute of Physics, Eötvös University, Pázmány P. s. 1/A, Budapest, H-1117, Hungary*

²*Institute for Theoretical Physics and HAS Research Group, Eötvös University, Pázmány P. s. 1/A, Budapest, H-1117, Hungary*

(Received 21 September 2011; accepted 2 March 2012; published online 4 April 2012)

Internal waves generated by surface perturbations are studied in a two-layer fluid in the presence of two thin sills of equal height in the lower layer, both experimentally and numerically. Small amplitude surface waves are found to generate internal waves of large amplitude at the density interface in between the two sills. The largest amplitude internal waves appear if a resonance condition is fulfilled: if half of the wavelength of the internal wave of the period of the external perturbation fits into the distance between the two sills in the form of standing waves. The internal waves are then apparently nonlinear, nevertheless, the predictions of a linear theory for the resonance condition apply by taking into account a systematic change in the wavelength caused by nonlinearity, and the deviation from a sharp density interface. Interestingly, the shape of these internal waves is found to be nearly sinusoidal. A precise classification proves them to be cnoidal waves with a small elliptic parameter m . © 2012 American Institute of Physics. [<http://dx.doi.org/10.1063/1.3699062>]

I. INTRODUCTION

Internal waves play an essential role in a realm of processes related to environmental flows,^{1,2} and are subject of increasing current interest.^{3–5} An isolated bottom obstacle, such as a sill, is known to enhance the complexity of phenomena. Tidal flow over sills periodically excites waves, turbulence, and intense mixing,^{6–9} even solitary waves.¹⁰ Bottom sills play an important role in dissipating tidal energy.^{11,12} Rotational effects can be neglected in most cases because of the relatively small length scales of natural sills in shallow layers, nevertheless modeling of oceanic currents modified by extended bottom obstacles requires the consideration of Coriolis force as well.^{13,14}

An observational¹⁵ and various model studies^{16–19} indicate that flows in a two-silled fjord exhibit an enhanced complexity as a consequence of internal wave interactions. Here we are interested in how the presence of two obstacles of approximately the same height (which is close to that of the pycnocline) change the internal dynamics in a two-layer fluid responding to weak external excitations. According to our best knowledge, this is the first work in which both numerical and experimental approaches are applied to systematically analyze the effects of two sills, as a function of their distances. Purely numerical studies with linear stratification have already been carried out in Refs. 16 and 17, based on an earlier work.¹⁸

An earlier study in our laboratory²⁰ showed that *one sill* in the middle of a tank is able to excite marked internal waves along the pycnocline if a small-amplitude barotropic standing wave is present on the water surface. The results showed that – since the horizontal flow is blocked at the bottom by the thin sill – a strong shear arises and a localized Kelvin-Helmholtz-like wave pattern, a separation eddy emerges near the edge of the sill in the direction of the flow, which periodically

^{a)} Author to whom correspondence should be addressed. Electronic mail: vincze.m@lecco.elte.hu.

varies in time, as it is driven by the phase of the surface wave forcing. This periodic tumbling yields propagation of baroclinic waves of large amplitude (see Fig. 5 of Ref. 20). It is important to note that in the absence of a bottom obstacle no such barotropic-baroclinic energy transfer takes place; in that case the displacement of the interface inherits the phase and the amplitude of the free surface. An important observation of this work is that small amplitude vertical oscillations in the surface (caused, for example, by an external seiche^{21,22}) might determine the time scale of the internal dynamics. Similar bottom sill-driven internal wave excitation processes have already been observed in natural water bodies as well, see, e.g., Refs. 21 and 22.

For the present work, we modified our experimental setup by adding a *second sill* in order to study the collective wave phenomena that arise in the presence of two sources of internal waves. This is motivated by the expectation that between two sills standing waves can occur with antinodes at the two ends. Moreover, if the period of these internal waves happens to coincide with that of the surface driving, a *resonance* with a particularly large amplitude response might occur.

We present here both experimental and numerical evidence that this qualitative expectation is basically correct. Small amplitude surface waves are found to be amplified in the interface in between the two sills. The largest amplitude internal waves appear if half of the wavelength of the *internal* wave of the period of the *external* perturbation fits into the distance between the two sills. The internal waves are then strongly nonlinear. Their maximal amplitude is of the order of the water height of the lower layer, and this value is an order of magnitude larger than for sill distances away from the resonant value. The predictions of a linear theory are, nevertheless, found to apply if one takes into account a systematic change in the wavelength caused by nonlinearity and the deviation from a sharp density interface. A precise classification proves them to be cnoidal waves with a small elliptic parameter m .

The paper is organized as follows. Section II presents the experimental setup. A resonance condition based on a basically linear reasoning is given in Sec. III. After a discussion of data acquisition (Sec. IV), the experimental results are presented in Sec. V. Next, the numerical analysis of the same phenomenon is presented, and practically the same resonance effect is found when solving the Navier-Stokes equations in a Boussinesq approximation. The closing Sec. VII discusses the relation between the linear theory and reality. We find that the basic reason for the disagreement is the deviation of the linear shallow-layer wavelength and the one measured in the setup. When taking into account the scale change due to this difference, a remarkable good agreement is found between the linearly predicted and the observed still distance belonging to resonance. A nonlinear analysis based on cnoidal standing and travelling waves provides an additional confirmation of the results.

II. EXPERIMENTAL SETUP

The laboratory experiment was performed in a $L = 2.26$ m long rectangular tank made of glass. The width and height of the tank were 15 and 25 cm, respectively. The tank was filled up to $H = 14$ cm by stratified water with a sharp pycnocline at the height of $H_1 = 8$ cm. Because of this marked interface, the setup can be approximately thought of as a two-layer fluid system. The bottom layer was made up of salt solution with an average density of $\rho_1 = 1028$ kg/m³. Blue dye was also added to this layer in order to make the waves along the pycnocline visible for optical data acquisition and processing (see Sec. IV). The upper layer consisted of freshwater ($\rho_2 = 1000$ kg/m³), that was carefully layered on top of the bottom layer to the height of $H_2 = 6$ cm. The temperature differences were on the order of 0.1 K throughout the whole tank, therefore the effect of temperature on the density was considered negligible.

In the middle of the tank a 5 mm thick acrylic glass sill was placed to the bottom, with a width equal to that of the tank, and a height of $h = 8$ cm that coincided with the position of the undisturbed pycnocline. A second, identical sill was placed at a horizontal distance d from the first sill. The location of the second sill – our control parameter – varied in the interval of $d = [3; 45]$ cm for the different measurements, while the location of the first sill was fixed. At the surface, waves with a characteristic amplitude of ~ 0.3 cm were excited by a 80 cm long and 13 cm wide foam rubber

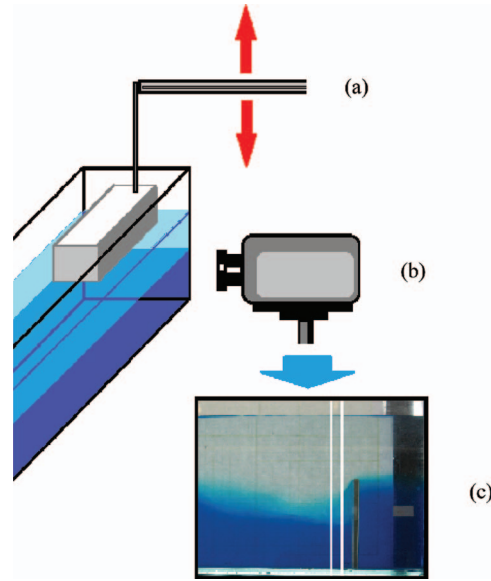


FIG. 1. Schematic drawing of the experimental setup with a computer-driven wave maker unit (a) and the camera mounted to the side of the tank (b). During data processing the video recordings were sliced to individual frames (c), and the pycnocline displacement in a selected pixel column (between the two white vertical lines of the figure) was detected as a function of time.

wave maker, mounted onto a computer-controlled traverse unit (a schematic drawing of the device is shown in Fig. 1). The period of this external barotropic (surface) wave forcing was set to $T = (6.6 \pm 0.01)$ s, that corresponds to a shallow water wavelength of $\lambda_{\text{ext}} = T\sqrt{gH} \approx 7.7$ m, more than three times as long as the tank itself.

III. RESONANCE CONDITION

Assuming that the waves in the system are in the linear regime (which is not necessarily true, considering their large amplitudes), the *internal* wavelength that corresponds to the period T of the surface forcing can be estimated as $\lambda_{\text{int}} = T\sqrt{g'H'} \approx 0.67$ m in shallow-layer approximation. Here $g' = g(\rho_1 - \rho_2)/\rho_2 \approx 0.3$ m/s² denotes the “reduced gravitational acceleration,” $H' = H_1H_2/H = 3.4$ cm represents the “reduced height,” and

$$c_1 \equiv \sqrt{g'H'} \approx 10.2 \frac{\text{cm}}{\text{s}} \quad (1)$$

is the phase velocity of linear internal waves in such a shallow-layer system (see, e.g., Ref. 23). With a qualitative reasoning, one would expect a resonance-like amplification of the internal wave amplitudes when the sill distance d equals to multiples of half a wavelength $\lambda_{\text{int}}/2$. Therefore, the condition of resonance is that the resonance length

$$D_{\text{res}} \equiv \frac{T \cdot c_1}{2} \quad (2)$$

becomes related to the sill distance d_{res} at resonance. In linear shallow-layer approximation, of course, $D_{\text{res}} = d_{\text{res}}$ holds.

Although the amplitude $A_0 = 3$ mm of the surface wave is small compared to the total water height of $H = 14$ cm and appears thus to be consistent with a linear approximation, the estimate $A' \approx A_0 g/g'$ for the amplitude of the internal waves valid within the same approximation²³ is already comparable to $H_1 = 8$ cm. This shows that the internal waves observed are in the strongly nonlinear regime. We investigated the dependence of barotropic-baroclinic energy transfer on d in this nontrivial setup.

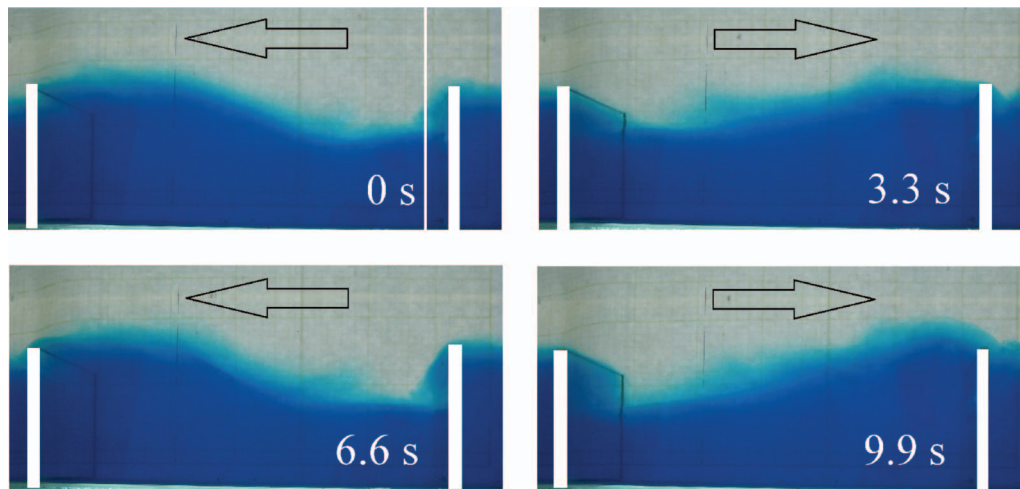


FIG. 2. Four snapshots of the flow pattern in the sill region for sill distance $d = 25$ cm. Time and the flow direction in the upper layer are indicated. The height of both sills is $h = 8$ cm.

IV. DATA ACQUISITION AND PROCESSING

The basic steps of data acquisition and processing are depicted in Fig. 1. Each experiment was recorded by a video camera that was placed to point perpendicularly to the sidewall of the tank in the region of the fixed sill. These video records were sliced (25 frames per second), and evaluated quantitatively. A vertical column of pixels was selected at a given horizontal position (shown as a single white vertical line in Fig. 2) nearby the fixed sill. The displacement of the pycnocline within this column was acquired by detecting the sharp change in the darkness level for each frame.

Fourteen experiments were carried out in the same two-layered fluid, each for different sill distance d . All of the obtained time series were smoothed by 7-point moving averaging. The testing of the reproducibility was crucial, as turbulent mixing during an experiment (and during the relocation of the sill) might alter the density profile and thus bias the results of the subsequent measurements. Therefore, after the completion of the 14 runs, a randomly selected 5 of them were repeated, and the obtained time series were compared with those of the previous runs. Not surprisingly, the largest relative reproducibility error corresponds to the experiment in which the largest amplitudes were observed. Nevertheless, even in this case the reproducibility is quite convincing, as seen in Fig. 3.

To obtain an appropriate measure of the intensity of barotropic-baroclinic transfer, we calculated the standard deviation of the pycnocline displacement for each d (all of the time series were of equal length of 44 s, or 1100 frames).

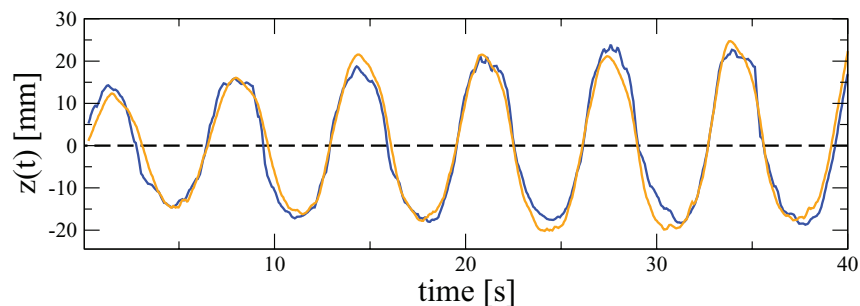


FIG. 3. Pycnocline displacement z versus time t for two different runs in the same setup ($d = 25$ cm).

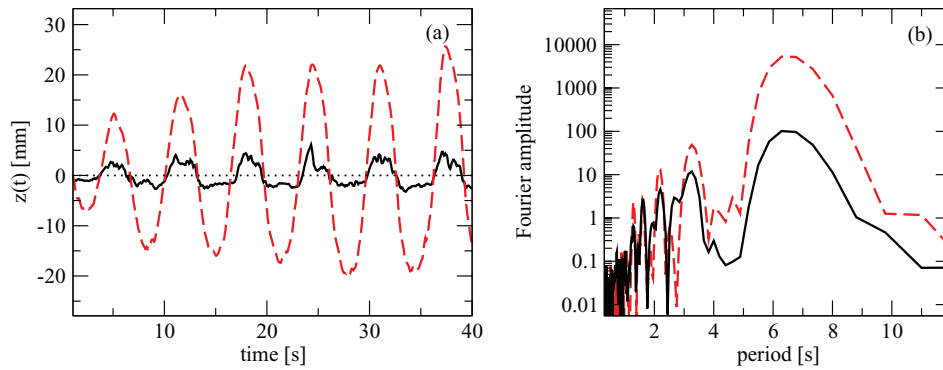


FIG. 4. The time series $z(t)$ of pycnocline displacement, (a) and its Fourier spectra (b) for $d = 9$ cm (solid curve) and 25 cm (dashed curve – red).

V. EXPERIMENTAL RESULTS

The time series $z(t)$ for sill distance $d = 9$ cm (solid black curve) and 25 cm (dashed curve – red) and their Fourier spectra are shown in Fig. 4. In both cases the largest Fourier amplitude appears at $T = 6.6$ s, the period of the external forcing. One can also notice an additional peak at 3.3 s which represents the first harmonic of the forcing, and another around 2.4 s. The main observation to be emphasized here is the following: while these smaller spectral amplitudes are on the same order of magnitude for both spectra, the peak at T is two orders of magnitude larger in the case of $d = 25$ cm, which clearly implies a resonance-like amplification.

The standard deviations for all of the experiments are shown in Fig. 5 as a function of the sill distance d . (The error bars were set to be twice as large as the greatest measured difference between the standard deviation σ value of an original experiment and that of its reproducibility test.) A typical resonance curve-like graph is obtained with a maximum around $d = 25$ cm. A three-parameter Lorentzian was fitted to these data in the form of

$$\sigma(d) = I \frac{\gamma^2}{(d - d_{\text{res}})^2 + \gamma^2}. \quad (3)$$

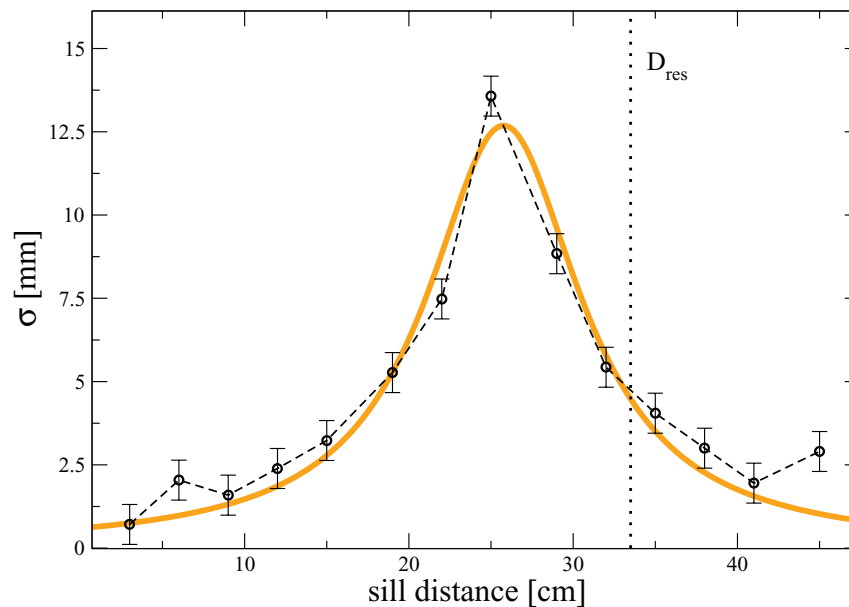


FIG. 5. The standard deviation σ values of the pycnocline displacement for the 14 experimental runs, as a function of the sill distance d . The dotted vertical line corresponds to $D_{\text{res}} = 33.5$ cm (details in the text).

The regression yielded the values of $d_{\text{res}} = (25.8 \pm 0.3)$ cm, $I = (12.7 \pm 0.2)$ mm, and $\gamma = (5.7 \pm 0.6)$ cm. The function is shown by a solid curve (orange) in Fig. 5.

The dotted vertical line in Fig. 5 represents the value of D_{res} (Eq. (2)). As mentioned in Sec. III, the linear shallow water wave theory and the “zero horizontal flux” boundary conditions predicted the maximal amplification to occur at $d = D_{\text{res}}$. Thus, a significant deviation from this theory is clearly visible, but the presence of a resonance-like behavior appears to remain.

VI. NUMERICAL SETUP AND RESULTS

In the numerical approach the two-dimensional Navier-Stokes equations were solved in nonhydrostatic Boussinesq approximation. An Arakawa-C grid²⁴ was used, which consisted of 201×26 equidistant cells, each sized $\Delta x \times \Delta z = 1.28$ cm \times 0.53 cm. These were chosen to correspond to the geometric parameters of the laboratory experiments. The kinematic viscosity ν was treated as an isotropic constant, of its usual molecular value of $\nu = 10^{-6}$ m²/s. Numerical solutions were obtained using the Advanced Ocean Modeling open-source software package, written in FORTRAN95 environment,²⁵ in which the system of partial differential equations is being solved with the method of successive over-relaxation, with slip boundary conditions at all solid boundaries. The numerical error was estimated by the divergence of the whole velocity field. A dimensionless divergence

$$\delta = T \left(\frac{\Delta u}{\Delta x} + \frac{\Delta w}{\Delta z} \right) \quad (4)$$

was used, where Δu is the horizontal and Δw the vertical velocity difference in neighbouring cells of horizontal and vertical size Δx and Δz , respectively. With the resolution used, the maximal value of δ was kept below 0.0015 at any time, indicating a reliable numerical accuracy.

The driving acceleration f was generated by a surface sine wave, with a period of $T = 6.6$ s and an amplitude of $A_0 = 3$ mm, a wave corresponding to the driving used in the experiments, in the form of

$$f = -g \frac{2\pi}{L} A_0 \sin \left(2\pi \frac{x}{L} \right) \cos \left(2\pi \frac{t}{T} \right), \quad (5)$$

where L (m) is the length of the tank and x represents the horizontal location. (For the simulations we took $L = 2.57$ m, but we note, that the actual value does not play a role, if it is large enough.) The initial density of the fluid is chosen as a function of the height z as follows:

$$\rho(z) = \rho_2 + \frac{\Delta\rho}{2} \left[1 + \tanh \left(\frac{H_1 - z}{l} \right) \right]. \quad (6)$$

$\rho_2 = 1000$ kg/m³ is the reference density, $\Delta\rho = 28$ kg/m³ the density difference between the two layers, $h = H_1$ is the height of the lower layer and specifies the position of the pycnocline, and $l = 1$ cm parametrizes the thickness of the gradient region. The latter corresponds to an approximately 3 cm thick regime around the pycnocline, where the density profile is nearly linear and changes about 3% (see shade color coding in Figure 6). The height of the lower layer $H_1 = 8$ cm and the upper layer $H_2 = 6$ cm were chosen to be the same as in the experiment.

The program created a data file in which the density values in each grid point were saved in every 0.6 s. A cell at a vertical location $z = H_1$ was selected from the horizontal region between the two sills so that it was in 2 grid point horizontal distance from the “fixed” sill. This distance was selected in order to yield an appropriate comparison with the experimental results for which the pycnocline displacement was evaluated at a similar vicinity of the sill (see the white vertical lines in Figs. 2 and 6). The density values of this selected cell were extracted and the pycnocline displacement as a function of time was stored for each different sill distance.

An example is shown in Figure 7 for $d = 25$ cm (dashed curve – red) and $d = 9$ cm (black solid curve). One can see that, like in the experiment, the peak for $d = 25$ cm is essentially larger than for $d = 9$ cm. Again, a resonance-like behavior is observed. It is worth noting that in a numerical simulation of another setting with linear stratification, a similar resonance was found by Xing and

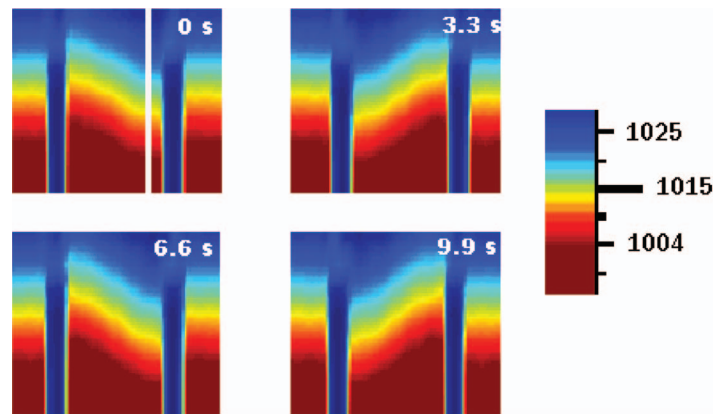


FIG. 6. A few snapshots of the simulation. Time instants in a steady state and the shade/color coding for the density [kg/m^3] distribution are indicated. The white vertical line marks the pixel column from where the pycnocline displacement time series was obtained. The height of both sills is $h = 8$ cm and the distance between them is $d = 27$ cm.

Davies.¹⁷ The resonance condition of the sill distance being a multiple of half of the wavelength of the internal waves, has been found there, too.

As in the experiment, the standard deviation σ was calculated for each time series. The $\sigma(d)$ values for all simulations are shown in Figure 8. Fitting a Lorentzian resonance curve in the form of Eq. (3), resulted in the values of $d_{\text{res}} = (26.9 \pm 0.3)$ cm, $I = (16.7 \pm 0.2)$ mm, and $\gamma = (4.1 \pm 0.4)$ cm. The function is shown by a solid curve (orange) in Fig. 8. The resonance appears at sill distance $d_{\text{res}} \approx 27$ cm, in fairly good agreement with the experimental results.

VII. DISCUSSIONS

Both in the case of experimental and numerical runs, the observed value of $d_{\text{res}} = (26 \pm 1)$ cm appeared to be significantly smaller than the theoretical $D_{\text{res}} = 33.5$ cm. The ratio of these quantities can be introduced as a “correction factor” α , that is found to be $\alpha = d_{\text{res}}/D_{\text{res}} \approx 0.8$. The question arises of what causes this deviation from the theory. One could argue that the difference is an effect of energy dissipation, analogously to the shift of resonant frequency that occurs if damping is applied to a linear oscillator. It is important to note that in the case of the numerical runs, only the viscous term of the Navier-Stokes equation could act as a source of such dissipation. As described in Sec. VI, the *molecular* value of viscosity ν was implemented, which clearly cannot be responsible for the observed magnitude of α , in itself. Yet, as seen, the numerical results are in agreement with the experiments, therefore we can rule out turbulent damping or boundary layer effects as the main

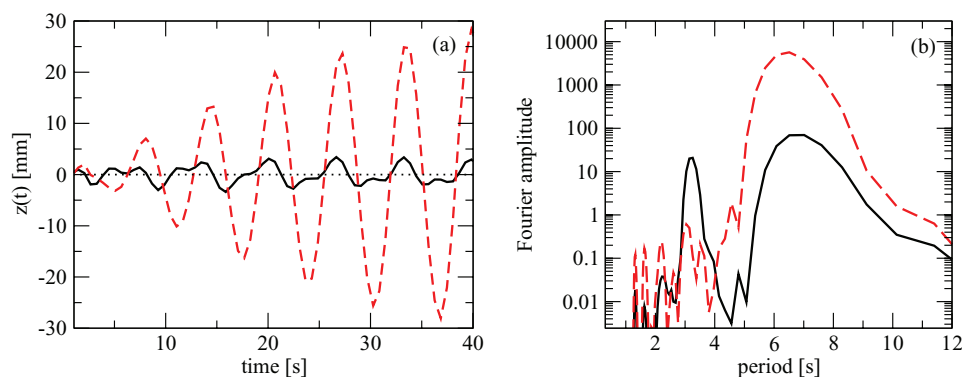


FIG. 7. The time series (a) and Fourier spectra (b) of the pycnocline displacement $z(t)$ obtained in the numerical simulation. $d = 25$ cm (dashed curve – red) and $d = 9$ cm (solid black curve) in both panels (cf. Fig. 4).

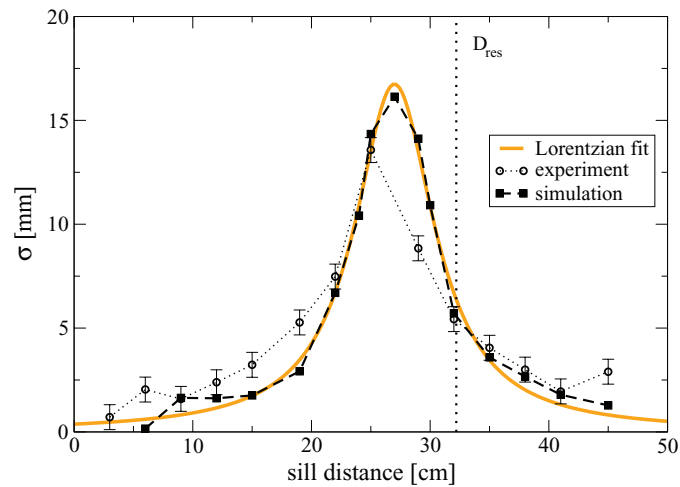


FIG. 8. The standard deviations for different sill distances d , obtained by numerical simulations (dashed curve) and by experiments (dotted curve). The Lorentzian fit to the numerical data is also shown (solid curve – orange). The dotted vertical line indicates the sill distance D_{res} for the first resonance mode according to the linear wave theory.

contributors to the shift, as these were not resolved by the program. Therefore, the remaining possible reasons for the difference could either be our inappropriate choice of the boundary conditions at the sills, or simply, that the linear two-shallow-layer approximation is not sufficient to describe this system.

In the first case, one could argue that the resonance condition (2) might not reflect the actual physics of the system accurately, as it is based on the assumption that the antinodes of the excited standing waves should be located at the sills. The horizontal velocity at the bottom vanishes in the vicinity of the vertical boundaries, which per se would force the pycnocline to stay horizontal and would hence yield an antinode in these regions. However, the horizontal flow in the upper layer could, in theory, cause a certain shear stress that might alter this waveform and lead to some sort of a mixed boundary condition. In order to test this hypothesis for our numerical setup, we calculated the square of the time-averaged absolute values of the pycnocline displacement $\langle |z(x, t)| \rangle^2$ as a function of the horizontal coordinate x for the grid columns between the two sills. The resulting pattern is shown in Fig. 9 for $d = 25$ cm onto which a function $f(x) = B \sin^2(x 2\pi/\lambda)$ was fitted (dashed line – orange). We note that for this fit $x = 0$ was set halfway between the two sills. The regression gives a wavelength of $\lambda = (51.0 \pm 3.5)$ cm that fairly coincides with $2d$. Therefore, we can state that the fluid indeed exhibits antinodes at the sills.

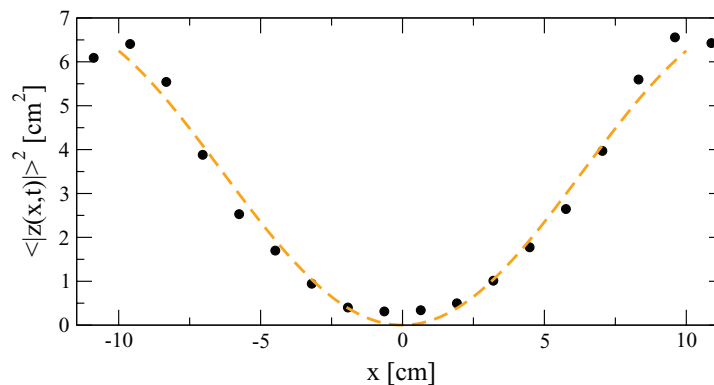


FIG. 9. Squared, time-averaged modulus $\langle |z(x, t)| \rangle^2$ of pycnocline displacement in the region between two sills from the numerical run for $d = 25$ cm, and the result of a fit of $f(x) = B \sin^2(x 2\pi/\lambda)$ (dashed line – orange).

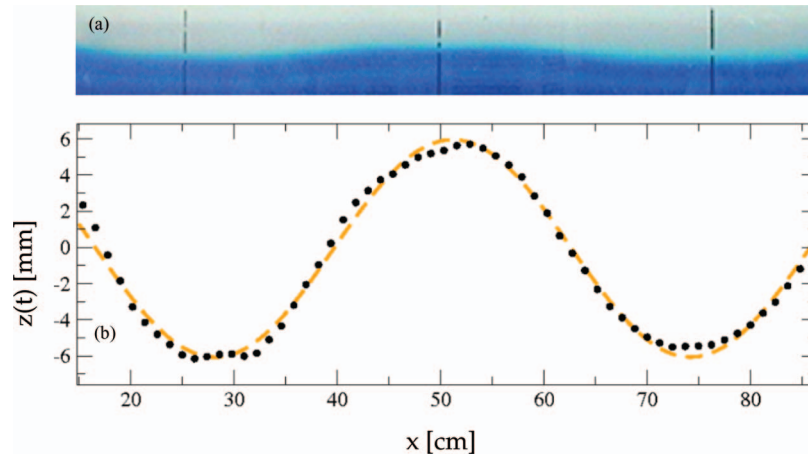


FIG. 10. (a) A photograph of the internal wave pattern with a period of $T = 6.6$ s in a single-sill control experiment. (b) The pycnocline displacement data (dots) obtained from the image in (a). The sinusoidal fit (dashed – orange) resulted in a wavelength of $\lambda_{\text{obs}} \approx 46$ cm.

This conclusion leads us to the second aforementioned option that the phase velocities of the internal waves in this setup could significantly differ from c_1 , and so could their wavelengths from the corresponding value. Knowing the period, we intended to measure the wavelength of a freely propagating internal wave along the pycnocline in a laboratory experiment, and compare the result with the prediction of the theory.

To carry out such a measurement, we needed a modified setup with only one sill located in the middle of the tank. In this control experiment, for the better observation of propagating waves, the length of the basin was extended to $L = 4.52$ m. The period of forcing remained $T = 6.6$ s. In the control setup, the linear theory yields $\lambda_{\text{theor}} = Tc_1 = (62 \pm 2)$ cm. Here the error originates from the uncertainty of the vertical position of the blurred density interface, and of the measurement of density. Photographs were taken of the pycnocline, such as the one shown in Fig. 10(a), and were processed as described in Sec. IV. Fitting a sinusoidal function $z(x) = C \sin(x 2\pi/\lambda + \phi)$ to the pycnocline displacement data (Fig. 10(b)) resulted in a wavelength of $\lambda_{\text{obs}} = (46 \pm 0.5)$ cm. We note, that approximately the same wavelength was observed in another control experiment with two sills (at $d = 25$ cm), too. We thus conclude, that d_{res} is basically set by the natural free wavelength of the system and is not modified by some “two-sill effect.” Interestingly, the accuracy of both this fit and the one of Fig. 9 indicates that despite of their large amplitudes, these internal waves are nearly sinusoidal. The ratio of the observed and theoretical wavelengths based on the linear theory gives $\lambda_{\text{obs}}/\lambda_{\text{theor}} = 0.75 \pm 0.04$, which is consistent with the value of the above defined correction factor α . This corresponds to the ratio of the phase velocities as well.

As already stated, the internal waves in our setup are of large amplitude, implying nonlinearity, which provides a possible explanation for the deviation from the linear theory. Because of the sinusoidal character of the waveforms, the best candidate to describe these internal waves is a *cnoidal* wave (see, e.g., Ref. 2) with a small elliptic parameter m . The governing two-layer Korteweg–de Vries (KdV) equation for the shape of the internal interface $\eta(x, t)$ reads as

$$\frac{\partial \eta}{\partial t} \pm c_1 \left(\frac{\partial \eta}{\partial x} + \frac{3}{2} \frac{H_2 - H_1}{H_1 H_2} \eta \frac{\partial \eta}{\partial x} + \frac{H_1 H_2}{6} \frac{\partial^3 \eta}{\partial x^3} \right) = 0. \quad (7)$$

Since the rescaling $\eta \rightarrow H_1 H_2 / (H_2 - H_1) \cdot \eta$, $x \rightarrow \sqrt{H_1 H_2} \cdot x$, $t \rightarrow \sqrt{H_1 H_2} / c_1 \cdot t$ leads to a dimensionless form, the same as for a homogeneous single-layer fluid,² using the well-known expressions for the wavelength λ and phase velocity c of a cnoidal wave, we obtain for the two-layer problem:

$$\lambda = \sqrt{\frac{16m}{6A} \frac{(H_1 H_2)^2}{H_2 - H_1}} K(m), \quad (8)$$

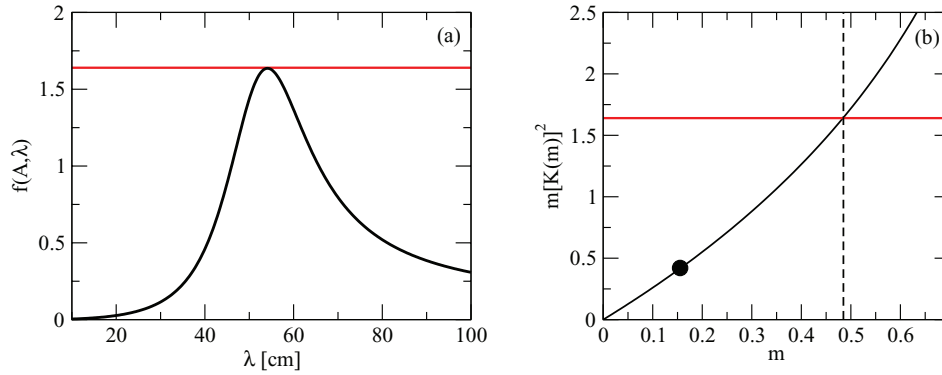


FIG. 11. (a) The dimensionless parameter $f(A, \lambda)$ of (11) corresponding to the observed wave amplitudes, as a function of wavelength with $H_1 = 8$ cm, $H_2 = 6$ cm. (b) The right-hand side of Eq. (11), as a function of the elliptic parameter m (black solid curve). The upper bound of $f(A, \lambda)$ is marked by a horizontal line (red) in both panels. The parameter value corresponding to the travelling internal wave of the control experiment (black dot) is also shown.

and

$$c = c_1 \left(1 + \frac{2A}{m} \frac{H_2 - H_1}{H_1 H_2} \left(1 - \frac{m}{2} - \frac{3}{2} \frac{E(m)}{K(m)} \right) \right). \quad (9)$$

Here A is the amplitude of the internal wave, m denotes the aforementioned elliptic parameter, and $K(m)$ and $E(m)$ are the complete elliptic integrals of the first and second kind, respectively, of elliptic modulus $k^2 = m$. Note that the wave height is $2A$ in this notation.

Using the observation that the σ of Eq. (3) is proportional to the wave amplitude A , we obtain for the λ dependence of the observed amplitudes between the two sills

$$|A(\lambda)| = A_m \frac{\gamma^2}{(\lambda/2 - d_{\text{res}})^2 + \gamma^2}. \quad (10)$$

Here we apply the fact that the wavelength is set by the sill distance as $\lambda = 2d$. Parameter $A_m = 1.8$ cm represents the largest observed amplitude at resonance. Substituting Eq. (10) into Eq. (8), we obtain an expression for elliptic parameter m ,

$$f(A, \lambda) \equiv \frac{6|A(\lambda)|\lambda^2}{16} \frac{|H_2 - H_1|}{(H_1 H_2)^2} = mK^2(m). \quad (11)$$

The dimensionless function $f(A, \lambda)$ is plotted against λ , for $H_1 = 8$ cm, $H_2 = 6$ cm in Fig. 11(a) with a maximum found to be 1.63. The right-hand side as a function of m can be seen in Fig. 11(b), along with a horizontal line corresponding to this maximum. One can see from here that the range of elliptic parameters of the observed standing waves is $0 < m < 0.48$. The lower bound $m = 0$ describes a standard sinusoidal wave.

The cnoidal waveform for the maximum, $m = 0.48$ is shown in Fig. 12. It is remarkable that the deviation from the sinusoidal form is so minor even at this relatively large value of m .

The mechanisms that select the resonance amplitude are hidden in the interaction of nonlinear waves, the details of which are difficult to unfold. From the arguments above only a range of m can be determined. One might, however also consider the travelling internal wave of the control experiment, after removing one of the sills. Similar analysis for this wave yields $m = 0.155$, and this value is marked as a dot in Fig. 11(b). The wave shape is also plotted as a black solid curve in Fig. 12. From the velocity formula (9), we get $c/c_1 = 0.85$. This is fairly close to the correction factor $\alpha = 0.8$ obtained when comparing the naive linear theory with the observations. Thus, the travelling wave of the control experiment appears to be the one whose properties should be used when determining the resonance condition.

Finally, let us mention that, in view of the blurred feature of the density interface, the calculations can be repeated for $H_1 = 7.5$ cm, $H_2 = 6.5$ cm, and $H_1 = 8.5$ cm, $H_2 = 5.5$ cm. These limits set the

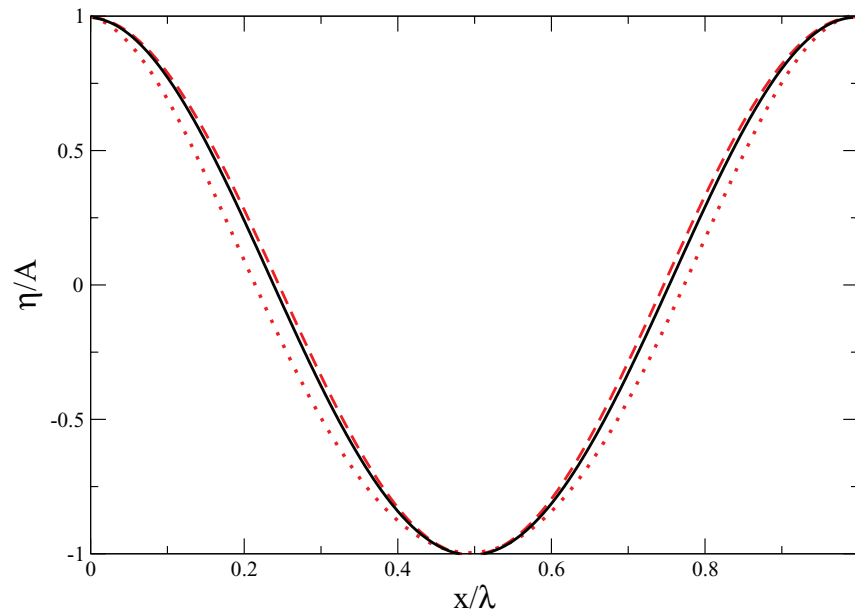


FIG. 12. The internal waveform obtained as a periodic solution of the two-layer KdV equation for amplitude $A = 1.8$ mm, layer heights $H_1 = 8$ cm, and $H_2 = 6$ cm, and elliptic parameter $m = 0.48$ (dotted curve – red). The internal wave then has the form $\eta(x)/A = 2/m \cdot [1 - m - E(m)/K(m)] + 2 \cdot \text{cn}^2[2K(m)x/\lambda, m]$, where cn denotes the Jacobi elliptic function (see, e.g., Ref. 2). A sinusoidal function $\cos(2\pi x/\lambda)$ is also shown (dashed curve – red). For comparison, the shape of the “free wave” characterized by $m = 0.155$ is also plotted (black solid line). Note that the deviations from the sine function are almost negligible.

uncertainty range for the predictions of the cnoidal theory. In particular, for the elliptic parameter of the travelling wave, we find with these layer configurations $m = 0.078$ and $m = 0.236$, respectively. Based on Eq. (9), we thus find that the cnoidal velocity c lies within the range of $c/c_1 = 0.8 \pm 0.1$, a value even closer to the correction factor α . These findings provide an evidence of the ubiquity of cnoidal waves, as the most general parametrization of waveforms, also observed in nature, ranging from the fully linear (simple harmonic) case at $m = 0$, to the fully nonlinear solitary wave solution at $m = 1$ (see, e.g., Ref. 26).

Our results raise the idea of a possible measuring method for field applications. There are several lakes, bays, and fjords, where the water body is strongly stratified. In such water bodies either conductivity or temperature measurements might work well to detect displacements of the internal density interface. The resonance effect should show up also when the obstacles do not sit on the bottom, but have a large enough height to hinder the weak horizontal currents excited by surface waves. Practically, one can think of a rectangular shape where the sidewalls can have a variable distance. As demonstrated, two vertical obstacles placed at the density interface work as an amplifier, and the measurement of the resonance peaks in internal oscillations provides a tool to detect and identify weak external oscillations.

ACKNOWLEDGMENTS

Useful discussions with P. Boschán and K. G. Szabó are acknowledged. This work was supported by the Hungarian Science Foundation under Grant No. OTKA NK72037 and NK100296. The project is also supported by the European Union and is co-financed by the European Social Fund (Grant agreement No. TAMOP 4.2.1./B-09/KMR-2010-0003).

¹ S. A. Thorpe, *The Turbulent Ocean* (Cambridge University Press, Cambridge, 2005).

² P. G. Baines, *Topographic Effects in Stratified Flows* (Cambridge University Press, Cambridge, 1995).

³ D. A. Cacchione, L. F. Pratson, and A. S. Ogston, “The shaping of continental slopes by internal tides,” *Science* **296**, 724–727 (2002).

- ⁴H. P. Zhang, B. King, and H. L. Swinney, "Resonant generation of internal waves on a model continental slope," *Phys. Rev. Lett.* **100**(24), 244504 (2008).
- ⁵B. King, M. Stone, H. P. Zhang, T. Gerkema, M. Marder, R. B. Scott, and H. L. Swinney, "Buoyancy frequency profiles and internal semidiurnal tide turning depths in the oceans," *J. Geophys. Res.* (to be published).
- ⁶D. M. Farmer and J. D. Smith, "Tidal interaction of stratified flow with a sill in Knight Inlet," *Deep-Sea Res., Part A* **27**, 239 (1980).
- ⁷W. R. Geyer and G. A. Cannon, "Sill processes related to deep water renewal in a fjord," *J. Geophys. Res.* **87**, 7985–7996, doi:10.1029/JC087iC10p07985 (1982).
- ⁸D. M. Farmer and H. J. Freeland, "The physical oceanography of fjords," *Prog. Oceanogr.* **12**, 147–220 (1983).
- ⁹L. Armi and D. M. Farmer, "The flow of Mediterranean water through the Strait and Gibraltar," *Prog. Oceanogr.* **21**, 1 (1988).
- ¹⁰D. Farmer and L. Armi, "The generation and trapping of solitary waves over topography," *Science* **283**, 188–190 (1999).
- ¹¹S. W. Tinnis and S. Pond, "Tidal energy dissipation at the sill of Sechart Inlet, British Columbia," *J. Phys. Oceanogr.* **31**, 3365–3373 (2001).
- ¹²L. Arneborg and B. Liljebladh, "Overturning and dissipation caused by baroclinic tidal flow near the sill of a fjord basin," *J. Phys. Oceanogr.* **39**, 2156–2174 (2009).
- ¹³P. D. Killworth, "Flow properties in rotating, stratified hydraulics," *J. Phys. Oceanogr.* **22**, 997–1017 (1992).
- ¹⁴K. G. Lamb, "Numerical experiments of internal wave generation by strong tidal flow across a finite amplitude bank edge," *J. Geophys. Res.* **99**, 843–864, doi:10.1029/93JC02514 (1994).
- ¹⁵A. M. Johnsson, J. A. M. Green, and A. Stigebrandt, "Baroclinic wave drag from two closely spaced sills in a narrow fjord as inferred from basin water mixing," *J. Geophys. Res.* **112**, C11002, doi:10.1029/2006JC003694 (2007).
- ¹⁶J. Xing and A. M. Davies, "Influence of multiple sills upon internal wave generation and the implications of mixing," *Geophys. Res. Lett.* **36**, L13602, doi:10.1029/2009GL038181 (2009).
- ¹⁷J. Xing and A. M. Davies, "On the interaction of internal tides over two adjacent sills in a fjord," *J. Geophys. Res.* **116**, C04022, doi:10.1029/2010JC006333 (2011).
- ¹⁸A. M. Davies, J. Xing, and A. J. Willmott, "Influence of open boundary conditions and sill height upon seiche motion in a gulf," *Ocean Dyn.* **59**, 863–879 (2009).
- ¹⁹M. W. Stacey and Y. Gratton, "The energetics and tidally induced reverse renewal in a two-silled fjord," *J. Phys. Oceanogr.* **31**, 1599–1615 (2001).
- ²⁰M. Vincze, P. Kozma, B. Gyüre, I. M. Jánosi, K. G. Szabó, and T. Tél, "Amplified internal pulsations on a stratified exchange flow excited by interaction between a thin sill and external seiche," *Phys. Fluids* **19**, 108108 (2007).
- ²¹R. Parsmar and A. Stigebrandt, "Observed damping of barotropic seiches through baroclinic wave drag in the Gullmar fjord," *J. Phys. Oceanogr.* **27**, 380 (1997).
- ²²D. Z. Zhu, H. Fouli, and Y. A. Okyere, "Exchange flow through an opening," *J. Hydraul. Res.* **40**, 341 (2002).
- ²³P. K. Kundu and I. M. Cohen, *Fluid Mechanics*, 4th ed. (Academic, Amsterdam, 2008).
- ²⁴A. Arakawa and V. Lamb, "Computational design of the basic dynamical processes of the UCLA general circulation model," *Methods Comput. Phys.* **17**, 173–265 (1977).
- ²⁵J. Kämpf, *Advanced Ocean Modelling* (Springer, Berlin/Heidelberg, 2009).
- ²⁶J. R. Apel, "A new analytical model for internal solitons in the ocean," *J. Phys. Oceanogr.* **33**(11), 2247–2269 (2003).